Proceedings article of the 5th Conference on Cryocrystals and Quantum Crystals in Wroclaw, Poland, submitted to *J. Low. Temp. Phys.* (2004).

Hydrogen-Helium Mixtures at High Pressure

Burkhard Militzer

Geophysical Laboratory, Carnegie Institution of Washington, 5251 Broad Branch Road, NW, Washington, DC 20015, USA

The properties of hydrogen-helium mixtures at high pressure are crucial to address important questions about the interior of Giant planets e.g. whether Jupiter has a rocky core and did it emerge via core accretion? Using path integral Monte Carlo simulations, we study the properties of these mixtures as a function of temperature, density and composition. The equation of state is calculated and compared to chemical models. We probe the accuracy of the ideal mixing approximation commonly used in such models. Finally, we discuss the structure of the liquid in terms of pair correlation functions.

PACS numbers: 62.50.+p, 02.70.Lq, 64.30.+t

1. INTRODUCTION

Hydrogen and helium are the two most abundant elements in giant planets. While Jupiter and Saturn are well characterized on the surface, many basic questions about its interior have not been answered[1]. Jupiter's surface composition has been measured *in situ* by the Galileo probe:[2] H 74.2% by weight, He 23.1%, and 0.027% heavier elements, which is enhanced compared to the protosolar composition: 0.015% heavier elements along with H 73.6% and He 24.9%. The abundance of heavy element in the interior and their distribution are not well characterized.[3] In particular, it is conversial whether Jupiter has a rocky core. The detection of a core in Jupiter may validate the standard model of giant-planet formation, nucleated capture of nebular hydrogen.[4] An alternative scenario was proposed by Alan Boss who suggested that giant planets form directly from spiral instabilities in protostellar disks.[5,6] Under this gravitational instability hypothesis, giant planets would not have a core, or at least a much smaller one.

Since there is no direct way to detect a core in Jupiter, one must instead refer to indirect measurements and to models for the planet interior. Such

models are constrained by the available observation data, in particular, the properties at the planet surface and the gravitational moments measured through fly-by trajectories. All models rely on an equation of state (EOS) of hydrogen-helium mixtures. However, the uncertainties in the available EOS are large and have not allowed one, among many other questions, to determine whether Jupiter has a core.

In this article, we present results from path integral Monte Carlo (PIMC) simulations[7] that enable us to study quantum many-body systems at finite temperature from first principles. In this simulation, hydrogen-helium mixtures are represented by an ensemble of electrons, protons and helium nuclei, each described by a path in imaginary time to incorporate quantum effects. The electrons are treated as fermions while exchange effects for the nuclei can be neglected for the considered thermodynamics conditions.

2. PATH INTEGRAL MONTE CARLO

The thermodynamic properties of a many-body quantum system at finite temperature can be computed by averaging over the density matrix, $\hat{\rho} = e^{-\beta \hat{H}}, \beta = 1/k_{\rm B}T$. Path integral formalism[8] is based on the identity,

$$e^{-\beta \hat{H}} = \left[e^{-\frac{\beta}{M}\hat{H}}\right]^M \tag{1}$$

where M is a positive integer. Insertion of complete sets of states between the M factors leads to the usual imaginary time path integral formulation, written here in real space,

$$\rho(\mathbf{R}, \mathbf{R}'; \beta) = \int \ldots \int d\mathbf{R}_1 \ldots d\mathbf{R}_{M-1}\, \rho(\mathbf{R}, \mathbf{R}_1; \tau) \ldots \rho(\mathbf{R}_{M-1}, \mathbf{R}'; \tau) \tag{2}$$

where $\tau = \beta/M$ is the time step. Each of the M steps in the path now has a high temperature density matrix $\rho(\mathbf{R}_k, \mathbf{R}_{k+1}; \tau)$ associated with it. The integrals are evaluated by Monte Carlo methods. The density matrix for bosonic and fermionic systems can be obtained by projecting out states of corresponding symmetry. In PIMC, one sums up different permutations P,

$$\rho_{\rm b/f}(\mathbf{R}, \mathbf{R}'; \beta) = \frac{1}{N!}\sum_{\mathcal{P}} (\pm 1)^{\mathcal{P}} \rho(\mathbf{R}, \mathcal{P}\mathbf{R}'; \beta) = \frac{1}{N!}\sum_{\mathcal{P}} (\pm 1)^{\mathcal{P}} \int\limits_{\mathbf{R}\rightarrow\mathcal{P}\mathbf{R}'} d\mathbf{R}_t\, e^{-U[\mathbf{R}_t]}. \tag{3}$$

For bosons, this is essentially an exact numerical algorithm that has found many applications.[7] For fermions, the cancellation of positive and negative contributions leads to numerically unstable methods, which is known as the

fermion sign problem. Ceperley showed that this problem can be solved by introducing the *restricted path* approximation,[9,10]

$$\rho_f(\mathbf{R}_0,\mathbf{R}';\beta) \approx \frac{1}{N!}\sum_{\mathcal{P}}(-1)^{\mathcal{P}}\int_{\substack{\mathbf{R}_0\to\mathcal{P}\mathbf{R}'\\ \rho_T(\mathbf{R}(t),\mathbf{R}_0;t)>0}} d\mathbf{R}_t\ e^{-U[\mathbf{R}(t)]} \quad , \tag{4}$$

where one only samples path $\mathbf{R}(t)$ that stay within the positive region of a *trial* density matrix, $\rho_T(\mathbf{R}(t),\mathbf{R}_0;t) > 0$. This procedure leads to an efficient algorithm for fermionic systems. All negative contributions to diagonal matrix elements are eliminated.[11] Contrary to the bosonic case, the algorithm is no longer exact since it now depends on the approximations for the trial density matrix. However, the method has worked very well in many applications.[12,13] For ρ_T, one can use the free particle or a variational density matrix.[14] In the results presented here, the high temperature density matrix was taken as a product of exact pair density matrices,

$$\frac{\rho(\mathbf{R},\mathbf{R}';\tau)}{\rho_0(\mathbf{R},\mathbf{R}';\tau)} = \left\langle e^{-\int_0^\tau dt\sum_{i<j}V(\mathbf{r}_{ij})}\right\rangle_{\mathbf{R}\to\mathbf{R}'} = \left\langle\prod_{i<j}e^{-\int_0^\tau dtV(\mathbf{r}_{ij})}\right\rangle_{\mathbf{R}\to\mathbf{R}'} \tag{5}$$

$$\approx \prod_{i<j}\left\langle e^{-\int_0^\tau dtV(\mathbf{r}_{ij})}\right\rangle_{\mathbf{r}_{ij}\to\mathbf{r}'_{ij}} \equiv e^{-\sum_{i<j}u(\mathbf{r}_{ij},\mathbf{r}'_{ij};\tau)}, \tag{6}$$

where $\rho_0(\mathbf{R},\mathbf{R}';\tau)$ is the free particle density matrix and $u(\mathbf{r}_{ij},\mathbf{r}'_{ij};\tau)$ is the pair action for paths initially separated by $\mathbf{r}_{ij}$ and finally at time τ by $\mathbf{r}'_{ij}$. An approximation is introduced by assuming that the different pair interactions can be averaged by independent Brownian random walks that are denoted by brackets $\langle\ldots\rangle$. This approach is efficient but not exact, and therefore puts a limit on the imaginary time step τ in many-body simulations. The pair action, u, can be computed by different methods.[15–17] The following simulation results were derived with $N_e = 32$ electrons and the corresponding number of protons, N_p, and helium nuclei $N_{\rm He}$ to obtain a neutral system ($N_e = N_p + 2N_{\rm He}$) with helium fraction $x \equiv 2N_{\rm He}/N_e$. Periodic boundary conditions are applied. As imaginary time discretization, we employ $\tau = 0.079$. (Atomic units of Bohr radii and Hartrees will be used throughout this article.)

The electrons are treated as fermions with fixed spin. We use variational nodes to restrict the paths and have therefore extended the approach in Ref. [14] to mixtures. The nuclei are also treated as paths but their exchange effects are not relevant here.

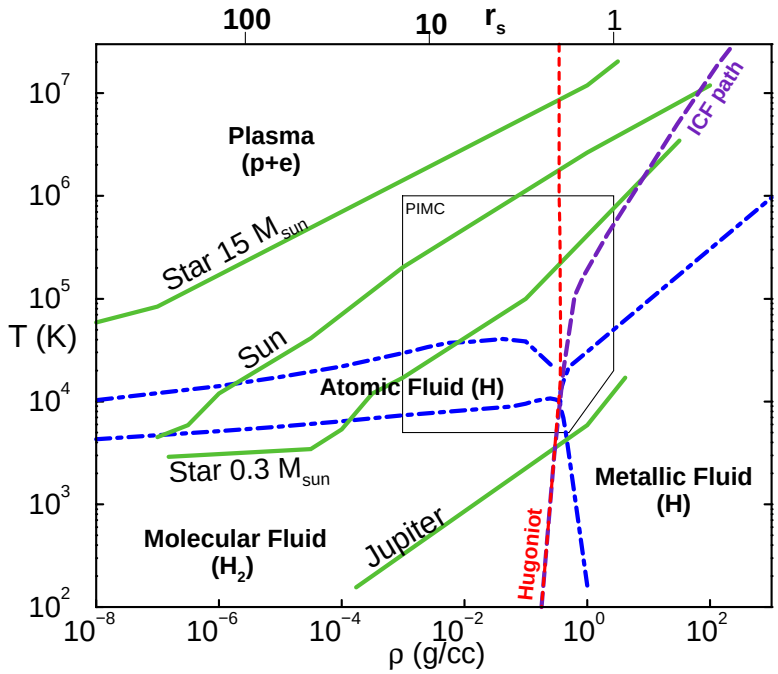

Fig. 1. Density-temperature phase diagram of hot dense hydrogen. The blue dash-dotted lines separate the molecular, the atomic, the metallic, and the plasma regime. The green solid lines are isentropes for Jupiter and stars with 0.3, 1, and 15 solar masses. Single shock Hugoniot states as well as the inertial confinement fusion path[18] are indicated by dashed lines. The thin solid line show ρ-T conditions of PIMC simulations.

3. PHASE DIAGRAM OF HOT DENSE HYDROGEN

Figure 1 shows the high temperature phase diagram of dense hydrogen beginning with the fluid and reaching up to a highly ionized plasma state. The figure includes the isentropes for Jupiter and low mass stars[19] and indicates the thermodynamic conditions, at which PIMC simulations have been applied.[20,21,13] We are now going to use these simulation results to characterize hot dense hydrogen from a path integral perspective.

At low density and temperature, one finds a fluid of interacting hydrogen molecules. A PIMC snapshot for $T = 5\,000\,\mathrm{K}$ and $r_s = 4.0$ is shown in Fig. 2. The proton paths are very localized due to their high mass. Their spread can be estimated from the de Broglie thermal wavelength, $\lambda_d^2 = \hbar^2\beta/2\pi m$. The electron paths are more spread out but they are localized to some extent since two electrons of opposite spin establish the chemical bond in the hydrogen

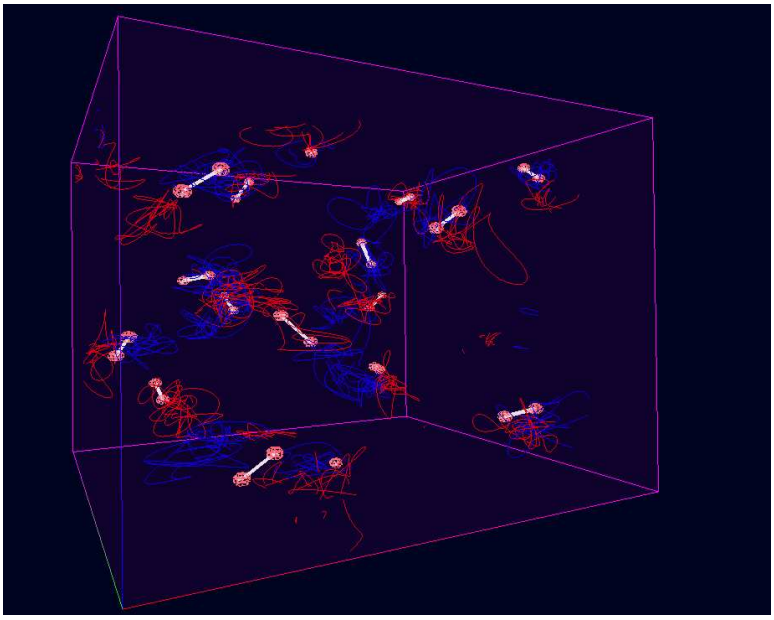

Fig. 2. Snapshot from PIMC simulations of pure hydrogen in the molecular regime at $T = 5\,000\,\mathrm{K}$ and $r_s = 4.0$. The pink spheres denote the protons. The bonds (white lines) were added as a guide to the eye. The electron paths are shown in red and blue [light and dark gray] depending on their spin state.

molecule.

If the temperature is raised from 5000 to 10^6 K, hydrogen undergoes a smooth transition from a molecular fluid though an atomic regime and finally to a two-component plasma of interacting electrons and protons. Many-body simulations at even higher temperatures are not needed since analytical methods like the Debye-Hückel theory work well. PIMC with explicit treatment of the electrons can also be applied to temperatures below $5\,000\,\mathrm{K}$ but groundstate methods are then more practical since excitation become less relevant and the computational cost scale with the length of paths like T^{-1}.

A detailed analysis of the chemical species present in the low density regime ($r_s \geq 2.6$) is given in Ref. 20. With decreasing density, one finds that the degree of molecular dissociation increases since the atomic state has higher entropy. For the same reason, one observes that the degree of atomic ionization increases with decreasing density. All these low-density effects can be well characterized by analytical models based on approximate free energy expressions for atoms, molecules and ionized particles.[22–25] In

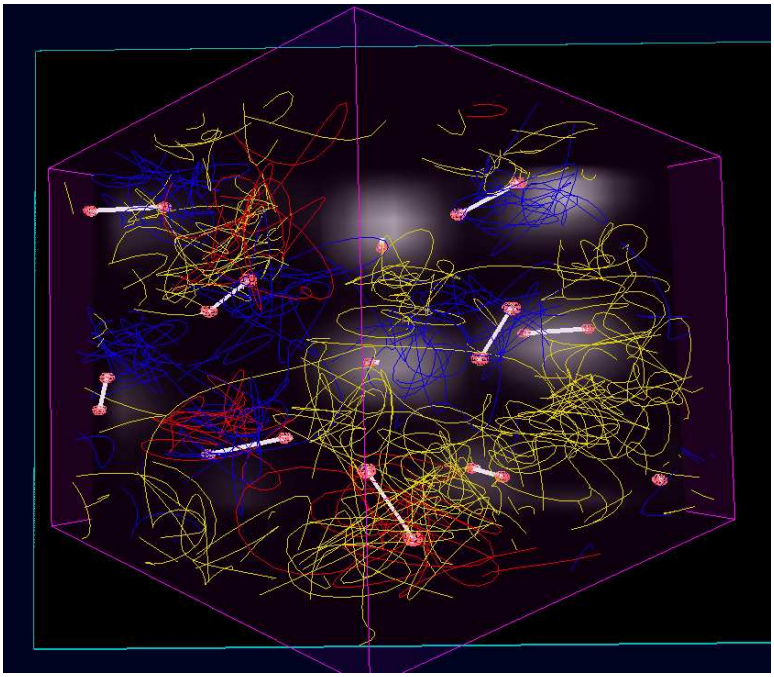

Fig. 3. Deuterium in the dense molecular regime ($T = 5\,000\,\mathrm{K}$ and $r_S = 1.86$) Due to the density increase compared to Fig. 2 (see details there), the electron paths permute with a rising probability (shown as yellow [light gray] lines) but are still localized enough to form a bond between the two protons in the molecule. The electron density average over many electron configurations is indicated in gray color on the blue rectangles.

this regime, one also finds reasonably good agreement between for the EOS derived from PIMC and chemical models.[20]

If the density is increased at $T = 5\,000\,\mathrm{K}$, one finds an intermediate regime of strongly interacting molecules (Fig. 3). Some electron paths exchange with neighboring molecules indicating the importance of fermionic effects. However, the electrons are still localized enough to provide a sufficient binding force for the protons.

If the density is increased further from $r_s = 1.86$ to 1.60, this binding force is lost due to further delocalization of the electrons (Fig. 4). Almost all electrons are now involved in long exchange cycles indicating a highly conducting, metallic state. No binding forces of the protons can be observed. One can therefore conclude that hydrogen metallizes in dissociated, or atomic form, a conclusion that is consistent with DFT simulations[26–29]. If the density is increased further, the electrons form a rigid neutralizing background and one recovers the limit of a one-component plasma of protons. If

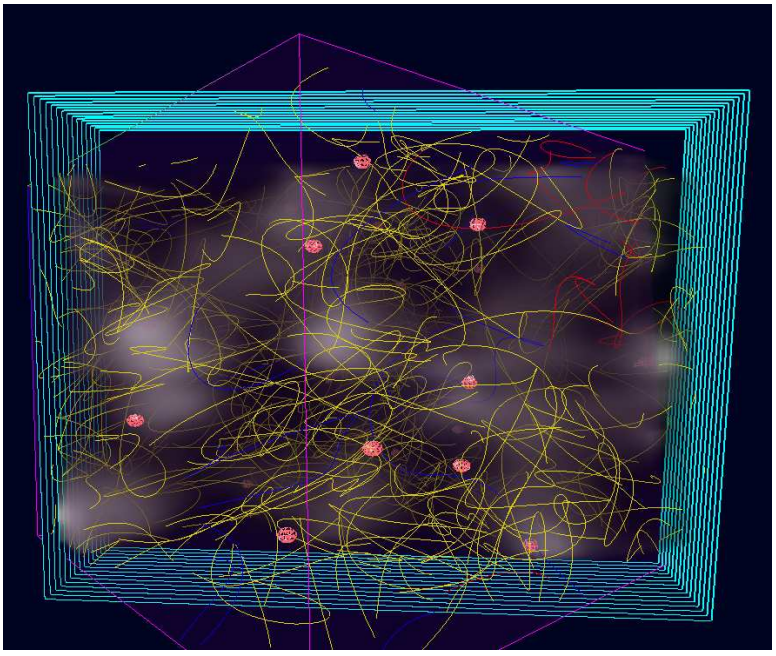

Fig. 4. Deuterium in the metallic regime characterized by unpaired protons and a gas of degenerate electrons. The snapshot was taken from a PIMC simulation at $T = 6\,250\,\mathrm{K}$ and $r_s = 1.60$. The electron paths are delocalized and exchange frequently (see description of Fig. 3).

the temperature is increased, the electron paths get shorter and shorter, the degree of electron degeneracy decreases gradually and one recovers the limit of a two-component plasma at high temperature.

The nature of the molecular-metallic transition has not yet been determined with certainty. A large number of analytical models[30] predict a first order transition, others do not.[23] PIMC simulation with free particle nodes by W. Magro *et al.*[31] showed an abrupt transition characterized by a region $\left.\frac{dP}{dT}\right|_V < 0$ for r_s=1.86. Later work by B. Militzer[32] using more accurate variational nodes did not show such a region for r_s=1.86. Whether PIMC simulations with variational nodes predict a gradual molecular-metallic transition for all temperatures, or if the region of an abrupt transition has shifted to lower, not yet accessible, temperatures has not been determined. However, recent density functional molecular dynamics simulations by various authors predict a first order transition below $5\,000\,\mathrm{K}$.[26–29]

There was a lot of recent interest focused on the hydrogen EOS because of the *unexpectedly high compressibility* inferred from the laser-driven shock wave experiment by Da Silva *et al.*[33] and Collins *et al.*[34] using the Nova

laser at Lawrence Livermore National Laboratory. The measurements indicated that hydrogen could be compressed to about 6-fold the initial density rather than 4-fold as indicated by the Sesame model.[35,36] Even though the temperatures and pressures reached in shock experiments are higher than those in the giant planets these measurements are crucial here since they represent the only way to distinguish between different EOS models at high temperature.

The Nova results challenged the existing understanding of high P-T hydrogen and triggered many new experimental and theoretical efforts. Different chemical models gave rise to very different predictions[30,23,37] ranging from 4-fold compression as suggested in[35,36] to 6-fold as predicted by the Ross model.[38] While the accuracy of chemical models did not allow any conclusive predictions, first principle simulations from PIMC[20,39] as well as from density functional molecular dynamics[40,28,29] consistently predict a lower compressibility of about 4.3.

Since then there have been many attempts to resolve this discrepancy but the most important contributions came from new experiments by Knudson *et al.*[41–43] at Sandia National Laboratory. Instead of a laser drive, they used magnetically driven shock waves in combination with bigger samples. They found a significantly lower compressibility quite similar to predictions from first principles methods. The new results are also supported by a third set of experiments by Russian investigators using spherically converging shock waves.[44,45]

4. HYDROGEN-HELIUM MIXTURES

Due to importance for astrophysical applications, EOS models for hydrogen-helium mixtures have been studied for quite some time. The most widely used EOS was derived by Saumon, Chabrier and van Horn (SCH).[19] Like previous chemical models, it is based on a hydrogen and a helium EOS that combined using an ideal mixing rule.

Following the discussion of the hydrogen EOS above, we are now analyzing the second ingredient: the EOS of helium. Given its low abundance in giant planets, helium is not expected to be present in very high concentration. However, Stevenson[46] has proposed that the hydrogen-helium mixture could phase separate under certain high pressure conditions. As a result, helium droplets would form and fall as rain towards planet core. The associated release of latent heat would delay the cooling process of the planet. This was suggested as one possible explanation of why standard models predict Saturn to cool at a much faster rate than is observed.[47] In order to detect

hydrogen-helium phase separation one needs an EOS of pure helium that we will now discuss.

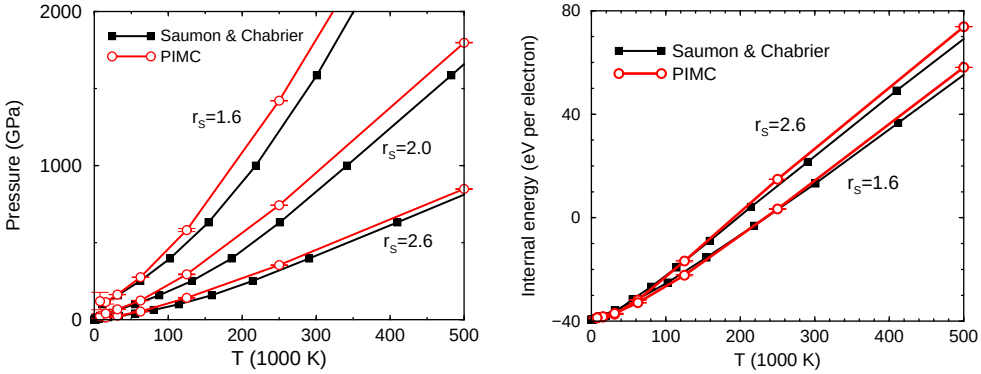

Fig. 5. Equation of state comparison for pure helium showing the pressure (left) and the internal energy (right) for different density as derived from path integral Monte Carlo simulations and the chemical model by Saumon, Chabrier, and van Horn.[19]

Figure 5 shows an EOS comparison of our PIMC calculations with the SCH model. One finds that the pressure is underestimated by SCH and that the deviations increase with density. The internal energy at high temperature is also underestimated. The analysis suggests a more careful treatment of the helium ionization states is needed to improve the chemical model.

To conclude the comparison with chemical models, we test one more assumption that is generally made: the ideal mixing hypothesis. We performed a large number of PIMC calculations of fully interacting hydrogen-helium mixtures at a fixed density of $r_s = 1.86$ for various temperatures and mixing ratios. The resulting correction to ideal mixing is given by,

$$\Delta f_{\rm mix} = f(x) - (1-x)\, f(x=0) - x\, f(x=1)\,. \tag{7}$$

Figure 6 shows that the corrections to pressure, $\Delta P_{\rm mix}$, increase with decreasing temperature reaching 10% for 15 625 K. In the considered temperature interval, the corrections to the internal energy are largest for 31 250 K which can be explained by the different ionization states of the two fluids that lead to larger error if ideal mixing is assumed.

Finally, we discuss pair correlation functions, $g(r)$, for hydrogen-helium mixtures,

$$g(r) \equiv \frac{\Omega}{N^2} \left\langle \sum_{i \neq j} \delta(\mathbf{r} - \mathbf{r}_{ij}) \right\rangle \,. \tag{8}$$

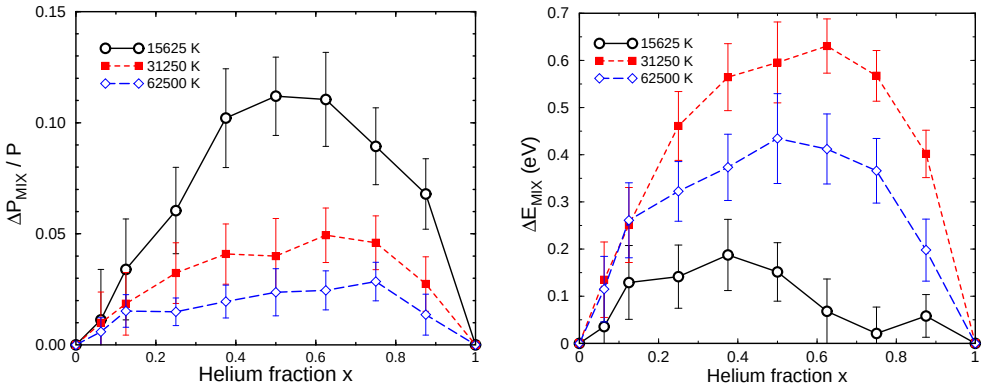

Fig. 6. Excess mixing pressure $\Delta P_{\rm mix}$ and internal energy per electron $\Delta E_{\rm mix}$ are shown for a hydrogen-helium mixture at $r_s = 1.86$. Path integral Monte Carlo results are shown for several temperatures. The mixing is performed at constant density. $\Delta E_{\rm mix}$ is largest for T=31 250 K because at this temperature the two end members are characterized by very different degrees of ionization.

$g(r)$ functions are a standard tool to characterize the short-range correlation of particles in liquids. In Fig. 7, we compare the correlation functions for pure hydrogen, a x=50% mixture, and pure helium at fixed temperature (15 625 K) and density ($r_s = 1.86$). Changes in the pair correlations are now discussed as a function of helium concentration. The electron-proton $g(r)$ shows a strong peak at the origin due to the Coulomb attraction. The peak is not affected when 50% helium is added to a pure hydrogen sample. Similarly, the correlation between electrons and helium nuclei is not altered by the presence of protons.

The electron-electron correlation depends strongly on spin. For pairs with parallel spin, exchange effects lead to a strong repulsion. The resulting $g(r)$ function does not depend much on whether helium is present or not. The correlation function between pairs of antiparallel spins, on the other hand, is strongly affected by the presence of helium nuclei. In the helium atom, two electrons with opposite spin are attracted to the core, which indirectly leads to the observed increase in the electron-electron $g(r)$.

It is interesting to note that proton-proton $g(r)$ changes with the helium concentration but the correlation of helium nuclei does not. With increasing presence of helium, a peak in the proton-proton $g(r)$ appears at $r = 1.4\,a_0$ which indicates the formation of H_2 molecules. Adding helium nuclei leads to the localization of a fraction of the electrons. The available space in combination with the reduced electronic exchange effects then leads to the

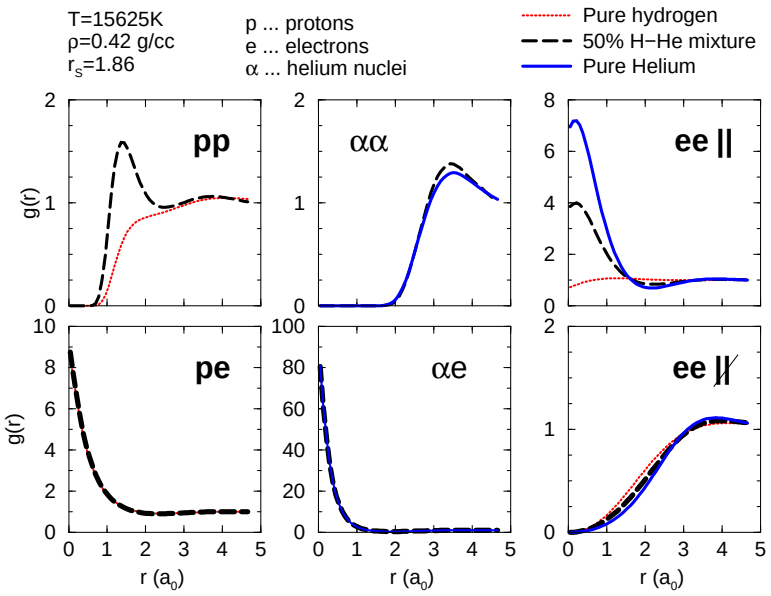

Fig. 7. Comparison of different pair correlation functions, $g(r)$, from three PIMC simulations at $r_s = 1.86$ and 15 625 K: pure hydrogen (red dotted lines), a $x = 50\%$ mixture (black dashed lines) and pure helium (blue solid lines). The six graphs show $g(r)$ for different pairs of protons (p), electrons (e) and helium nuclei (α). For electrons, pairs with antiparallel (upper right) and with parallel (lower right) spins are distinguished.

formation of hydrogen molecules which are not present in pure hydrogen at the same temperature and density.

5. CONCLUSIONS

The discussion in this article centered on the phase diagram of hot dense hydrogen. The first PIMC results for hydrogen-helium mixtures were presented here, and the accuracy of existing helium EOS models as well as the commonly used ideal mixing rule were analyzed. This analysis revealed substantial inaccuracies in existing EOS models. These uncertainties prevent us from making reliable models for the interior of giant planets and from drawing conclusions about their formation mechanism, either nucleated capture of nebular hydrogen[4] or gravitational instability driven formation in protostellar disks.[5,6]

An improved EOS will also yield a better characterization of the 120

extrasolar giant planets that have been discovered so far using radio velocity measurements.[48] In particular the mass-radius relationship obtained from transit extrasolar giant planets[49] will allow one to draw conclusions about the heavy element abundance in those planets. The metallicity of a planet relative to its central star constrains the role of accretion of planetesimals in the planet's formation.

ACKNOWLEDGMENTS

The author thanks W. Hubbard and D. Stevenson for useful discussions and D. Saumon for providing us with the SCH EOS.

REFERENCES

1. T. Giullot, W. B. Hubbard, D. J. Stevenson, and D. Saumon. In F. Bangenal *et al.* editor, *Jupiter: The Planet, Satellites and Magnetosphere*. Cambridge University Press, 2004.
2. J. J. Fortney and W. B. Hubbard. *Icarus*, 164:228, 2003.
3. D. Saumon and T. Guillot. *Astrophys. J.*, 609:1170, 2004.
4. J. J. Lissauer. *Annu. Rev. Astron. Astrophys.*, 31:129, 1993.
5. A. P. Boss. *Science*, 276:1836, 1997.
6. A. P. Boss. *Astrophys. J.*, 610:456, 2004.
7. D. M. Ceperley. *Rev. Mod. Phys.*, 67:279, 1995.
8. R. P. Feynman. *Phys. Rev.*, 90:1116, 1953.
9. D. M. Ceperley. *J. Stat. Phys.*, 63:1237, 1991.
10. D. M. Ceperley. Path integral Monte Carlo for fermions. In K. Binder and G. Ciccotti, editors, *Monte Carlo and Molecular Dynamics of Condensed Matter Systems*. Editrice Compositori, Bologna, Italy, 1996.
11. B. Militzer, E.L. Pollock, and D. Ceperley, 2004.
12. C. Pierleoni, D.M. Ceperley, B. Bernu, and W.R. Magro. *Phys. Rev. Lett.*, 73:2145, 1994.
13. B. Militzer and E. L. Pollock. *Phys. Rev. Lett.*, 89:280401, 2002.
14. B. Militzer and E. L. Pollock. *Phys. Rev. E*, 61:3470, 2000.
15. R. G. Storer. *J. Math. Phys.*, 9:964, 1968.
16. E. L. Pollock. *Comp. Phys. Comm.*, 52 :49, 1988.
17. K. E. Schmidt and M. A. Lee. *Phys. Rev. E*, 51:5495, 1995.
18. J. Lindl. *Phys. Plasmas*, 2 (11):3933, 1995.
19. D. Saumon, G. Chabrier, and H. M. Van Horn. *Astrophys. J. Suppl.*, 99:713, 1995.
20. B. Militzer and D. M. Ceperley. *Phys. Rev. Lett.*, 85:1890, 2000.
21. B. Militzer and D. M. Ceperley. *Phys. Rev. E*, 63:066404, 2001.
22. D. Saumon and G. Chabrier. *Phys. Rev. A*, 46:2084, 1992.
23. F.J. Rogers. *Astrophys. J.*, 352:689, 1990.

24. W. Ebeling, W.D. Kraeft, and D. Kremp. *Theory of Bound States and Ionisation Equilibrium in Plasma and Solids*. Ergebnisse der Plasmaphysik und der Gaselektronik, Band 5. Akademie-Verlag, Berlin, 1976.
25. H. Juranek, R. Redmer, and Y. Rosenfeld. *J. Chem. Phys.*, 117:1768, 2002.
26. S. Bagnier, P. Blottiau, and J. Clarouin. *Phys. Rev. E*, 63:015301, 2000.
27. S. Scandolo. *Proc. Nat. Ac. Sci.*, 100:3051, 2003.
28. M. P. Desjarlais. *Phys. Rev. B*, 68:064204, 2003.
29. G. Galli S. A. Bonev, B. Militzer. *Phys. Rev. B*, 69:014101, 2004.
30. D. Beule, Werner Ebeling, and Andreas Förster. *Phys. Rev. B*, 59:14177, 1999.
31. W. R. Magro, D. M. Ceperley, C. Pierleoni, and B. Bernu. *Phys. Rev. Lett.*, 76:1240, 1996.
32. B. Militzer. PhD thesis, University of Illinois at Urbana-Champaign, 2000.
33. I. B. Da Silva, P. Celliers, G. W. Collins, K. S. Budil, N. C. Holmes, W. T. Jr. Barbee, B. A. Hammel, J. D. Kilkenny, R. J. Wallace, M. Ross, R. Cauble, A. Ng, and G. Chiu. *Phys. Rev. Lett.*, 78:483, 1997.
34. G. W. Collins, L. B. Da Silva, P. Celliers, D. M. Gold, M. E. Foord, R. J. Wallace, A. Ng, S. V. Weber, K. S. Budil, and R. Cauble. *Science*, 281:1178, 1998.
35. G. I. Kerley. In J. M. Haili and G. A. Mansoori, editors, *Molecular Based Study of Fluids*, page 107. American Chemical Society, Washington DC, 1983.
36. G. I. Kerley. Equations of state of hydrogen and deuterium, 2003. Sandia Report, SAND2003-3613, Sandia National Laboratory, Albuquerque, NM 87185.
37. H. Juranek and R. Redmer. *J. Chem. Phys.*, 112:3780, 2000.
38. M. Ross. *Phys. Rev. B*, 58:669, 1998.
39. B. Militzer, D. M. Ceperley, J. D. Kress, J. D. Johnson, L. A. Collins, and S. Mazevet. *Phys. Rev. Lett.*, 87:275502, 2001.
40. T. J. Lenosky, S. R. Bickham, J. D. Kress, and L. A. Collins. *Phys. Rev. B*, 61:1, 2000.
41. M. D. Knudson, D. L. Hanson, J. E. Bailey, C. A. Hall, J. R. Asay, and W. W. Anderson. *Phys. Rev. Lett.*, 87:225501, 2001.
42. M. D. Knudson, D. L. Hanson, J. E. Bailey, C. A. Hall, and J. R. Asay. *Phys. Rev. Lett.*, 90:035505, 2003.
43. M. D. Knudson, D. L. Hanson, J. E. Bailey, C. A. Hall, J. R. Asay, and C. Deeney, 2004. submitted to *Phys. Rev. B*.
44. S.I. Belov, G.V. Boriskov, A.I. Bykov, R.I. Il'kaev, N.B. Luk'yanov, A.Y. Matveev, O.L. Mikhailova, V.D. Selemir, G.V. Simakov, R.F. Trunin, I.P. Trusov, V.D. Urlin, V.E. Fortov, and A.N. Shuikin. *JETP Lett.*, 76:443, 2002.
45. G.V. Boriskov, A.I. Bykov, R.I. Il'Kaev, V.D. Selemir, G.V. Simakov, R.F. Trunin, V.D. Urlin, V.E. Fortov, and A.N. Shuikin. *Dokl. Phys.*, 48:553, 2003.
46. D.J. Stevenson and E.E Salpeter. *Astrophys. J. Suppl.*, 35:239, 1977.
47. J. J. Fortney and W. B. Hubbard. *Astrophys. J.*, 608:1039, 2004.
48. G.W. Marcy, R.P. Butler, D.A. Fischer, and S.S. Vogt. In D. Deming and S. Seager, editors, *Scientific Frontiers in Research on Extrasolar Planets*. ASP Conference Series, 2002.
49. T. Brown, D. Charbonneau, R. Gilliland, R. Noyes, and A. Burrows. *ApJ*, 552:699, 2001.